33. Benton E V et al., in *Proc. 7th Intern. Colloq. Corpuscular Photography and Visual Solid Detectors, Barcelona, 1970*, p. 423
34. Cross W G, Tommasino L *Health Phys.* **15** 196 (1968)
35. Tommasino L, Klein N, Solomon P *Nucl. Track Detection* **1** 63 (1977)
36. Harvey J R, Weeks A R *Nucl. Tracks Radiat. Meas.* **6** 201 (1982)
37. Tommasino L "Electrochemical etching of damaged track detectors by H.V. pulse and sinusoidal waveform", International Rept. Lab. Dosimetria e Standardizzazione (Rome: CNEN Casaccia, 1970)
38. Wang H, in *Proc. 12th Intern. Conf. on Ultra-Relativistic Nucleus-Nucleus Collisions, Heidelberg, May 1996*
39. Astafyeva N M et al., in *Proc. 6th Conf. on the Intersections of Particle and Nuclear Physics, 1997*, p. 269
40. Di Liberto S, Ginobbi P *Nucl. Instrum. Meth.* **147** 75 (1977)
41. Abmayr W et al. *Nucl. Instrum. Meth.* **147** 79 (1977)
42. Schott J U, Schopper E, Staudte R *Nucl. Instrum. Meth.* **147** 63 (1977)
43. Niwa K, Hoshino K, Niu K, in *Proc. of the Intern. Cosmic Ray Symp. on High Energy Phenomena* (Tokyo: Cosmic Ray Lab., Univ. 1974) p. 149
44. Feinberg E L, Kotelnikov K A, Polukhina N G *Fiz. Elem. Chast. Atom. Yadra* **35** 763 (2004) [*Phys. Part. Nucl.* **35** 409 (2004)]
45. Boos E G et al., in *Experiments at CERN in 1996* (Geneva, 1996) p. 122
46. Chernavskaya O D et al., in *Proc. 28th Intern. Conf. on High Energy Physics, Proc., Warsaw, 1996*, Vol. 1, p. 941
47. Dobrotin N A et al. *Izv. Ross. Akad. Nauk Ser. Fiz.* **63** 485 (1999)
48. Dremin I M et al. *Phys. Lett. B* **499** 97 (2001); hep-ph/0007060
49. Polukhina N G, Doctoral Thesis, Phys. Math. Sci. (Moscow: Lebedev Physical Institute, 2006)
50. Aleksandrov A B, PhD Thesis (Moscow: Lebedev Physical Institute, 2009)
51. Dremin I M et al., in *Proc. of the 4th Rencontres du Vietnam, 2000*, p. 531
52. Dremin I M *Nucl. Phys. A* **767** 233 (2006); hep-ph/0507167
53. Apanasenko A V et al. (RUNJOB Collab.) *Astropart. Phys.* **16** 13 (2001)
54. Apanasenko A V et al. (RUNJOB Collab.) *Izv. Ross. Akad. Nauk Ser. Fiz.* **65** (3) 433 (2001)
55. Kamioka E et al. (RUNJOB Collab.) *Adv. Space Res.* **26** 1839 (2001)
56. Publichenko P A et al. (RUNJOB Collab.), in *Proc. of 27th Intern. Cosmic Ray Conf. August 2001 Germany, Hamburg 2001* Vol. 6, p. 2131
57. Hareyama M et al. (RUNJOB Collab.) *Nucl. Instrum. Meth. Phys. Res. A* **512** 553 (2003)
58. Furukawa M et al. (RUNJOB Collab.) *Proc. 28th ICRC* **4** 1885 (2003)
59. Kovalenko A D et al. *Few-Body Syst. Suppl.* **14** 241 (2003)
60. Adamovich M I et al. *Pis'ma Fiz. Elem. Chast. Atom. Yadra* (2) 29 (2003)
61. Adamovich M I et al. *Yad. Fiz.* **67** 533 (2004) [*Phys. Atom. Nucl.* **67** 514 (2004)]
62. Adamovich M I et al., nucl-ex/0301003
63. Bradnova V et al. *Acta Phys. Slovaca* **54** (4) 351 (2004)
64. Andreeva N P et al., Preprint No. P1-2004-91 (Dubna: JINR, 2004)
65. Andreeva N P et al. *Yad. Fiz.* **68** 484 (2005) [*Phys. Atom. Nucl.* **68** 455 (2005)]
66. Tumendelger Ts et al., Preprint No. P1-99-247 (Dubna: JINR, 1999)
67. Krivopustov M I et al., Preprint No. P1-2000-168 (Dubna: JINR, 2000)
68. Kotelnikov K A et al., Preprint No. 25 (Moscow: Lebedev Physical Institute, 2001)
69. Azarenkova I Yu et al. *Prib. Tekh. Eksp.* (1) 66 (2004) [*Instrum. Exp. Tech.* **47** 58 (2004)]
70. Apacheva I Yu et al., in *Proc. 54th Int. Workshop on Nuclear Spectroscopy and Structure of the Atomic Nucleus* (Belgorod, 2004) p. 276
71. Abdurazakov A A et al. *Atlas Spektrov Elektronov Vnutrennei Konversii Neitronodefitsitnykh Radioaktivnykh Nuklidov v Oblasti A = 131–172* (An Atlas of the Spectra of Internal Conversion Electrons of Neutron-deficit Radioactive Nuclides in the Region of A = 131–172) (Tashkent: Uzbekiston, 1991)
72. Starkov N I, Doctoral Thesis, Phys. Math. Sci. (Moscow: Lebedev Physical Institute, 2010)
73. Belovitskii G E et al. *Izv. Ross. Akad. Nauk Ser. Fiz.* **70** 650 (2006)
74. Powell C F, Fowler P H, Perkins D H *The Study of Elementary Particles by the Photographic Method* (London: Pergamon Press, 1959) [Translated into Russian (Moscow: IL, 1962)]
75. Aleksandrov A B et al., Preprint No. 29 (Moscow: Lebedev Physical Institute, 2005)
76. Markov M A *Neitrino* (Neutrino) (Moscow: Nauka, 1964)
77. Acquafredda R et al. *JINST* **4** P04018 (2009)
78. Agafonova N et al. (OPERA Collab.) *Phys. Lett. B* **691** 138 (2010)
79. Ginzburg V L et al. *Dokl. Ross. Akad. Nauk* **402** 472 (2005) [*Dokl. Phys.* **50** 283 (2005)]
80. Strutinsky V M *Nucl. Phys. A* **95** 420 (1967)
81. Ginzburg V L *Usp. Fiz. Nauk* **169** 419 (1999) [*Phys. Usp.* **42** 353 (1999)]
82. Zel'dovich Ya B *Zh. Eksp. Teor. Fiz.* **38** 1123 (1960) [*Sov. Phys. JETP* **11** 812 (1960)]
83. Bisnovatyi-Kogan G S, Chechetkin V M *Usp. Fiz. Nauk* **112** 263 (1979) [*Sov. Phys. Usp.* **22** 89 (1979)]
84. Kramarovskii Ya M, Chechev V P *Sintez Elementov vo Vselennoi* (Synthesis of Elements in the Universe) (Moscow: Nauka, 1987)
85. Perron C, Maury M *Int. J. Radiat. Appl. Instrum. D* **11** (1–2) 73 (1986)
86. Perron C, Bourot-Denise M *Int. J. Radiat. Appl. Instrum. D* **12** 29 (1986)
87. Donnelly J et al., in *Proc. of the 26th Intern. Cosmic Ray Conf., 1999*, OG1.1.30
88. Westphal A J et al. *Nature* **396** 50 (1998)
89. Binns E V et al. *Astrophys. J.* **346** 997 (1989)
90. Fowler P H et al. *Astrophys. J.* **314** 739 (1987)
91. Aleksandrov A B et al. *Usp. Fiz. Nauk* **180** 839 (2010) [*Phys. Usp.* **53** 805 (2010)]
92. Aleksandrov A B et al., in *Proc. 32nd Intern. Cosmic Ray Conf., Beijing, August 2011*
93. Ashitkov V D et al. *Kratk. Soobshch. Fiz. FIAN* (10) 22 (2010) [*Bull. Lebedev Phys. Inst.* **38** (10) 297 (2011)]

PACS numbers: 74.25.Ha, 74.25.Op, **74.50.+r**, **74.72.–h**, 74.72.Hs
DOI: 10.3367/UFNe.0182.201206h.0669

High-temperature superconductors in high and ultrahigh magnetic fields

S I Vedeneev

1. Introduction

High-temperature (or high-T_c) superconductors (T_c being the superconducting transition temperature) compose a family of materials with a generic structural peculiarity which consists in the presence of relatively well-separated copper–oxygen (Cu–O) planes. They are also termed as cuprates. Some compositions in this family exhibit the highest T_c among all known superconductors. The current record is held at $T_c = 135$ K ($T_c = 165$ K if the sample is kept under pressure). High-temperature superconductivity results from doping a Mott insulator with charge carriers and exists in a narrow carrier concentration range. Figure 1 demonstrates a

S I Vedeneev P N Lebedev Physical Institute,
Russian Academy of Sciences, Moscow, Russian Federation
E-mail: vedeneev@sci.lebedev.ru

Uspekhi Fizicheskikh Nauk **182** (6) 669–676 (2012)
DOI: 10.3367/UFNr.0182.201206h.0669
Translated by E G Strel'chenko; edited by A Radzig

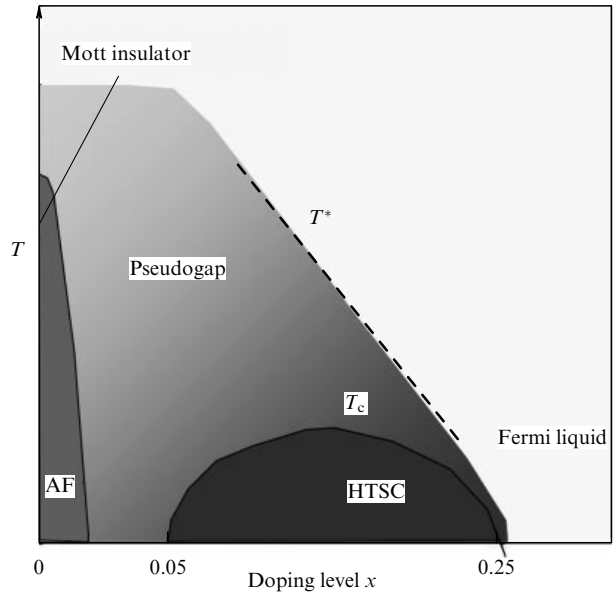

Figure 1. Cuprate phase diagram (AF denotes antiferromagnet).

typical phase diagram of a cuprate compound. The long-range antiferromagnetic order (at $T = 0$) disappears at a hole concentration $p \approx 0.03$ per Cu atom, and underdoped samples start superconducting at $p \approx 0.05$. The optimal doping level is one that maximizes T_c.

Cuprates of various compositions share a variety of generic features both in the normal and in the superconducting states, many of which have no explanation within the Bardeen–Cooper–Schrieffer (BCS) framework. Currently, no theory can consistently explain high-temperature superconductivity in cuprates. With the discovery of high-temperature superconductivity, the following three fundamentally crucial questions came to the fore:

— Do charge carriers form a Fermi liquid in the normal state?

— How do high T_c relate to the pseudogap, i.e., to normal state correlations that appear for $T^* > T_c$ or below T_c but above the upper critical field H_{c2}?

— What is the nature of the superconducting transition at T_c?

Of these, so far only the first question has been given a definitive answer. As for the other two, a number of explanatory models have been proposed, two of which have received particular attention. The first assumes that the appearance of pseudogap at temperatures above T_c is somehow the effect of antiferromagnetic ordering which develops in a high-temperature superconductor (HTSC) with zero (or low) charge carrier doping. The superconducting transition then follows the usual BCS scenario in which the superconducting gap closes and the macroscopic wave function vanishes, necessarily implying that a pseudogap state is inherently incompatible — and therefore competes — with d-wave superconductivity occurring in HTSCs. The second theory offers a phase disordering scenario in which thermally generated vortices violate long-range phase coherence, and the pair condensate loses phase rigidity but survives, at temperatures far above T_c, in a pseudogap state. Although these two states are expected to differ only slightly from each other, it is this difference which is fundamentally responsible for the superconducting pairing mechanism.

As research on HTSCs progressed, it became clear that their superconducting properties are, to a large extent, determined by their normal state properties which, like the former, are mostly anomalous and vary strongly with carrier concentration. Therefore, the study of the normal state conductivity of HTSC single crystals — including that between the layers — provides information on quasiparticle properties, which is of crucial importance for understanding the high-temperature superconductivity mechanism.

An unusual normal-state feature of an HTSC is that the 'metallic' temperature dependence of the resistivity ρ_{ab} along the CuO_2 (*ab* planes) layers coexists in it with the semiconductor-like resistivity ρ_c in the direction perpendicular to the CuO_2 layers (along the *c*-axis) (see, for example, Refs [1–3]). Note that the magnetic field suppression of superconductivity led to a $\log(1/T)$ divergence in the ρ_c versus temperature dependence at low temperatures [4]. This very marked difference in behavior between ρ_{ab} and ρ_c is likely to imply two-dimensional localization and incompatibility with the Fermi-liquid behavior [5]. At the same time, in the temperature range of semiconductor-like $\rho_c(T)$, many HTSC experiments have shown negative magnetoresistance along the *c*-axis, which was attributed by some to the closure of the pseudogap. These two observations, the semiconductor-like behavior of $\rho_c(T)$ and negative nagnetoresistance, have been discussed repeatedly within various models, including strongly attenuated tunneling along the *c*-axis; interlayer-scattering hopping conductivity; the reducing effect of superconducting fluctuations on the quasiparticle density of states, etc.

Of particular interest in relation to the physics of carriers in strongly correlated and disordered systems (of which HTSCs are an example) is the coexistence of superconductivity and localization. The latter can lead to a metal–insulator (M–I) transition in a metallic system [6]. The M–I transition has been observed in a number of underdoped HTSC compounds and involves a transition to the dielectric-like behavior of the resistivity $\rho_{ab}(T)$, which increases as $\log(1/T)$ without saturation (see, for example, Ref. [4] and references cited therein).

As for the pseudogap, which has been observed, in particular, in NMR, photoemission, and tunneling experiments on underdoped normal-state HTSCs, some authors [7–9] interpret it as a precursor of superconductivity and argue that thermal or quantum fluctuations in this state destroy superconducting phase coherence. For others, the pseudogap is not of a superconducting nature and can exist in the spin portion of the spectrum of excitations if these are divided into a spin and a charge part. However, spin lattice relaxation experiments have produced widely contradictory results concerning the spin gap dependence. It was shown by various authors that, depending on the particular HTSC system, the onset of the semiconducting behavior of $\rho_c(T)$ may either coincide or not coincide with the opening of the spin gap. There is currently no consensus as to the nature of the pseudogap, nor as to how it relates to superconductivity.

In many laboratories worldwide, research on layered Bi-based HTSCs were found to perform best in terms of the reproducibility of results. The superconducting transition temperature of a Bi cuprate is determined by how many (1, 2, or 3) two-dimensional CuO_2 planes reside in the unit cell. These HTSCs include $Bi_{2+x}Sr_{2-x}CuO_6$ (Bi2201) with $T_c = 0-13$ K, $Bi_{2-y}La_ySr_2CuO_6$ (Bi(La)2201) with $T_c = 0-35$ K, $Bi_2Sr_2CaCu_2O_8$ (Bi2212) with $T_c = 92$ K, and

$Bi_2Sr_2Ca_2Cu_3O_{10}$ (Bi2223) with $T_c = 115$ K. The crystal structure of layered Bi-based HTSCs along the c-axis comprises a system of identical Josephson internal contacts (junctions) in which one, two, or three neighboring CuO_2 layers are separated by $Bi_2Sr_2O_4$ layers acting as an insulating tunneling barrier. It is this layered structure which explains the very high anisotropy of the transport and magnetotransport properties of Bi-based HTSCs.

It is well known that as far as the electronic characteristics of metals are concerned, studies of their properties at low and ultralow temperatures are of particular importance. For simple (BCS) superconductors, such studies were conducted in magnetic fields that drove samples into the normal state, and because the critical magnetic fields H_{c2} of HTSCs are very high, strong (up to 30 T) and ultrastrong (above 30 T) magnetic fields were needed for low-temperature normal-state studies of their properties. However, as even early work showed, the Bi2201, Bi2212, and Bi2223 systems are all very similar in their basic properties. Because the values of H_{c2} in superconductors are proportional to T_c, the natural choice for transport and magnetotransport studies would be samples of a single-layer $Bi_2Sr_2CuO_6$ compound — a low-temperature phase of a Bi-HTSC, but, unfortunately, the stoichiometric composition of this cuprate is an insulator. This difficulty was overcome by partially replacing strontium with lanthanum in Bi(La)2201 single crystals or by using $Bi_{2+x}Sr_{2-x}CuO_{6+\delta}$ single crystals with an excess of bismuth. We used La-undoped Bi-excess Bi2201 single crystals in obtaining our main results, because the absence of alien metal (La) improved Bi2201 single crystals structurally. Furthermore, provided optimal doping, a permanent magnet (!) can be used to drive these single crystals into the normal state. Thus, studying Bi2201 also provided information on the properties of high-temperature HTSC phases.

Single crystals of $Bi_{2+x}Sr_{2-x}CuO_6$ and $Bi_2Sr_2CaCu_2O_8$ were grown and given their complete characterization at the P N Lebedev Physical Institute of the Russian Academy of Sciences (Moscow). Magnetic measurements were made at two laboratories in France: Grenoble High Magnetic Field Laboratory (Grenoble), and National Pulsed Magnetic Field Laboratory (Toulouse).

2. Normal-state resistance anisotropy in high-temperature superconductors

We used our previously developed method [10, 11] of the crystal free growth in a gaseous cavity from a KCl solution-melt to obtain high-quality single-crystalline $Bi_{2+x}Sr_{2-x}CuO_{6+\delta}$ in the doping range $0.09 < x < 0.7$, T_c range from 0 to 13 K, and a size range of (0.5–1.0) mm $\times$ (0.5 – 1.0) mm $\times$ (1 – 10) μm. The crystal quality was checked by measuring the dc resistivity and ac susceptibility using X-ray diffraction and electron microscopy techniques. The X-ray rocking curve half-width did not exceed 0.1° – 0.3° (depending on the crystal size). The composition microanalysis of the samples was made using a Philips CM-30 electron microscope attached to an X-ray spectrometer. The cation composition was measured at ten to forty points in various regions of the crystal, with a data spread of no more than 2%. Our Hall coefficient measurements on several crystals revealed a near linear Bi excess versus carrier concentration relation, which was used in subsequent work. It was found that the optimal doping for the Bi2201 system occurs when the number of carriers per copper atom is $p = 0.17$. We were able to plot the $p - T_c$ phase diagram for pure (La-undoped) Bi2201 compound over a doping range of $p = 0.09$–0.20.

We measured for the first time the temperature dependences of the resistivities $\rho_{ab}(T)$ and $\rho_c(T)$ and those of the magnetoresistivity $\rho_{ab}(H)$ and $\rho_c(H)$ in single crystals of Bi2201 cuprate for various doping levels ($T_c = 2.0 - 10.5$ K) and over a wide temperature range down to 20 mK. In Fig. 2, panels a–d display $\rho_{ab}(T)$ dependences obtained in a number of fixed magnetic fields for several samples with p values between 0.12 and 2.0 (to better show the low-temperature ρ_{ab} behavior, a semilog scale was used). Because the results obtained in the magnetic fields $H = 20.0$ T and $H = 27.5$ T are nearly identical, it reasonably follows that they indeed refer to the normal state. In two underdoped samples with a carrier concentration $p = 0.12$ (Fig. 2a) and 0.13 (Fig. 2b), as the temperature is decreased, the resistivity ρ_{ab} first goes through a minimum and then, at $T \approx 30$ K (Fig. 2a) and $T \approx 10$ K (Fig. 2b), increases as $\log(1/T)$ in keeping with the onset of localization [4, 13]. As noted above, Ono et al. [4] revealed in underdoped samples of Bi(La)2201 and $La_{2-x}Sr_xCuO_4$ (LSCO) that ρ_{ab} follows the $\log(1/T)$-like behavior at temperatures from 30.0 K to 0.3 K without low-temperature saturation. As can be seen from Figs 2a, b, however, ρ_{ab} in Bi2201 exhibits at ultralow temperatures $T = 0.04 - 0.2$ K and in very high magnetic fields a departure from the $\log(1/T)$ behavior. This departure has no relation to the proximity of the superconducting transition, because $\rho_{ab}(T)$ demonstrates identical behavior in 20 T and 27.5 T fields. Furthermore, the data for $H = 27.5$ T in Fig. 2b underlie those for $H = 20$ T. We interpret the onset of ρ_{ab} saturation as the suppression of localization by the imposed magnetic field.

On the contrary, $\rho_{ab}(T)$ for the $p = 0.16$ (Fig. 2c) and $p = 0.2$ (Fig. 2d) samples (slightly underdoped and overdoped, respectively) turns out to be constant at temperatures below 5 K, clearly pointing to metallic normal-state behavior. Most likely — and similar to Bi(La)2201 [4] — the metal–insulator transition in Bi2201 lies in the underdoped region

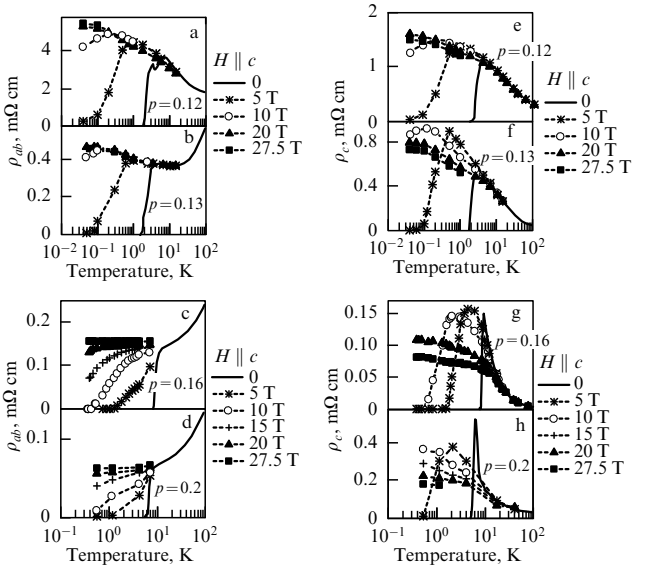

Figure 2. Semilog plots of the temperature dependences of ρ_{ab} (a–d) and ρ_c (e–h) for different fixed strengths of a magnetic field for one and the same set of samples with a carrier concentration p from 0.12 to 2.0 per Cu atom [12].

($p < 0.16$). As the carrier concentration increases, $\rho_{ab}(T)$ steadily changes its behavior from dielectric to metallic.

Figures 2e–h present the semilog plots of $\rho_c(T)$ for various fixed values of the magnetic field strength for the same samples as in Figs 2a–d with p falling between 0.12 and 2.0. A strong magnetic field prevents resistance from increasing with decreasing temperature, and $\rho_c(T)$ tends to saturate in slightly underdoped or overdoped single crystals. It is evident that as the carrier concentration increases, then, both for $\rho_c(T)$ and $\rho_{ab}(T)$, the $\log(1/T)$ normal-state behavior steadily changes to metallic behavior, the onset of this change shifting to higher temperatures with increasing p. Our data on $\rho_c(T)$ are in strong disagreement with the results measured on LSCO and Bi(La)2201 single crystals [5, 14], which depict a $\log(1/T)$ singularity in the normal state for $T \ll T_c$ (down to 0.66 K). In the view of the authors of these studies, the fact that the metallic ρ_{ab} behavior coexisting with the semiconducting behavior of ρ_c was an unambiguous indication of the non-Fermi-liquid nature of Bi(La)2201. However, as apparent from Figs 2e–h, we have no evidence for the $\log(1/T)$ singularity in underdoped Bi2201 single crystals at low temperatures, and the resistivity ρ_c of slightly underdoped and overdoped Bi2201 single crystals is nearly temperature-independent for $T < T_c$ at the strongest magnetic fields employed. This implies that in the low-temperature limit, $T/T_c \to 0$, charge transfer occurs by the same mechanism in the *ab* and *c* directions.

The resistivity anisotropy parameter ρ_c/ρ_{ab} is often used to characterize interlayer coupling in HTSCs. (In our experiments, this parameter reached 2.2×10^4 near T_c.) In previous work, the zero-field value of ρ_c/ρ_{ab} was strongly temperature-dependent, leading the previous authors to assume different charge transfer mechanisms for directions along and across the CuO_2 layers. Our measurements at low temperatures and in very strong magnetic fields showed that, for all doping levels, the normal-state value of ρ_c/ρ_{ab} is practically temperature-independent. The saturation of ρ_c/ρ_{ab} serves as a further indication of the similar three-dimensional nature of charge transport in all Bi2201 single crystals and arbitrarily strong magnetic fields.

3. Thermal conductivity of Bi2201 single crystals

As noted in Section 2, a major question in the physics of HTSCs reduces to the following: how valid Landau's Fermi-liquid theory is in describing the elementary excitations of the HTSC ground state. HTSCs fall into the category of doped Mott insulators with strong Coulomb repulsion (a feature not accounted for in the Fermi-liquid approach), and there is recent evidence [15] for the inadequacy of Fermi-liquid theory when applied to HTSC cuprates. How much this hinders the formation of quasiparticles in the zero-temperature limit can be established by measuring the normal-state heat conductivity at ultralow temperatures. This makes it possible to check the validity of the Wiedemann–Franz (WF) law, universal for Fermi liquids, which suggests that the electrical conductivity σ and the heat conductivity κ of quasiparticles are related through the universal constant $\kappa/\sigma T = L_0 = 2.44 \times 10^{-8}$ W Ω K^{-2}. Because the properties of HTSCs are strongly dependent on the doping level, of particular importance was to see to what extent varying the doping level violates the WF law in cuprates. Our choice for this study was Bi2201 single crystals because the available magnetic fields of up to 28 T were sufficient to transfer these samples to the normal state at temperatures down to 90 mK. These measurements were the first ever of their kind. Since no measurements had been made of heat conductivity at ultralow temperatures in such strong (> 15 T) magnetic fields, a special-purpose facility was designed and constructed by us. The same experiment measured the temperature dependence of sample resistivities, necessary for matching the electrical and thermal conductivity data. In solving the rather challenging task of measuring ultralow temperatures in strong fields in a vacuum, the Nanoway Company's (Finland) Coulomb blockade thermometer, a lattice system of one-electron tunnel junctions, was employed.

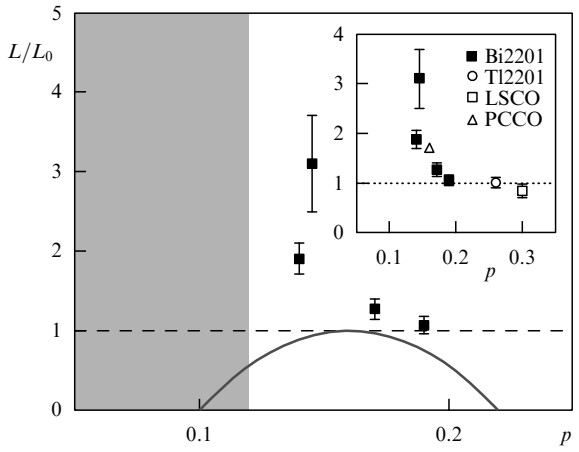

Figure 3. Experimental values of the Lorentz number $L = \kappa/\sigma T$ normalized to L_0 for four Bi2201 single crystals with different doping levels (black squares). The shaded region corresponds to an insulator. The inset shows our results together with similar data obtained by others on other cuprates ($Pr_{2-x}Ce_xCuO_4$, $Tl_2Ba_2CuO_6$, and $La_{2-x}Sr_xCuO_4$). The horizontal line exhibits the value of L/L_0 expected from the WF law [16, 17]).

It was found that for single-crystalline Bi2201 near the optimal doping level, $p = 0.17$, the linear (electronic contribution) term in the thermal conductivity temperature dependence is very close to the quantity governed by the WF law, identifying as fermions the elementary excitations that transfer charge and heat in optimally doped cuprates. The lower the doping level, the stronger the violation of the WF law in a sample. The linear term increased with temperatures, and at $p = 0.12-0.13$ was several times the WF value. Figure 3 shows as black squares the experimental values of the Lorentz number $L = \kappa/\sigma T$ (normalized to L_0) for four Bi2201 single crystal with different doping levels. The inset gives our results together with similar data obtained by other authors on $Pr_{2-x}Ce_xCuO_4$ (PCCO), $Tl_2Ba_2CuO_6$ (Tl2201), and LSCO cuprates. The value of L/L_0 expected from the WF law is shown as a horizontal line. The shaded region corresponds to the material occupying the insulating state. These results show conclusively that Fermi-liquid theory breaks down as an underdoped HTSC cuprate moves away from the optimal doping state and approaches the insulating state.

4. Upper critical field and its anisotropy in Bi2201 single crystals

Although the upper critical field $H_{c2}(0)$ is a major parameter in the realm of high-temperature superconductivity, there is still some uncertainty about its value and temperature dependence $H_{c2}(T)$. Because HTSCs have very high critical magnetic fields, the measurements were conducted at tem-

peratures close to T_c, and the values of $H_{c2}(0)$ were determined by extrapolating to zero temperature. The structural simplicity and low T_c make low-temperature phases of HTSCs an ideal choice for such studies. The first experiments on the single crystals of Tl2201 (T_c of about 20 K) [18] and films of Bi2201 (T_c of about 15 K) [19] in strong magnetic fields revealed that $H_{c2}(T)$ varies anomalously with temperature. As the temperature decreased, the magnetoresistance curves shifted to higher fields, but no saturation was observed. The values of $H_{c2}(0)$ greatly exceeded those expected from the slope of dH_{c2}/dT in the vicinity of T_c. None of the commonly accepted models could explain this exotic behavior of $H_{c2}(T)$.

Our study included a thorough investigation of the $H-T$ phase diagram for magnetic fields applied parallel and perpendicular to the conducting planes in Bi2201 single crystals. The measurements were made on slightly underdoped samples with a carrier concentration of $p = 0.15-0.16$ per copper atom and $T_c = 7-9$ K. Magnetoresistivity was measured by exposing the samples to constant (up to 28 T) and pulsed (up to 55 T) magnetic fields in a wide temperature range down to 40 mK and 0.4 K, respectively. Due to low T_c, the field strength of 52 T proved to be sufficient to suppress superconductivity at $T/T_c = 0.04$ in the parallel configuration. In pulsed magnetic fields, identical results were obtained for both the front (26 ms duration) and tail (110 ms duration) portions of the pulse, ruling out the possibility of a sample being heated by vortex currents. The resistive upper critical field H^*_{c2} corresponded to the field strength at which the resistance along the *c*-axis or *ab* plane reached the normal-state value for a given temperature. The curves in Figs 4a and b show, for various temperatures, the transition to the normal state of one Bi2201 single crystal in a magnetic field parallel to the *c*-axis and *ab*-plane, respectively. As seen from Fig. 4c, the experimental data for $H^*_{c2\perp ab}$ in magnetic fields perpendicular to the *ab* plane (points at the bottom) are described well in the temperature range $T/T_c = 0.04-1.00$ by the Werthamer–Helfand–Hohenberg (WHH) theory based on the orbital mechanism of superconductivity suppression in simple superconductors. For magnetic fields parallel to the *ab* plane, the $H^*_{c2\|ab}(T)$ data for $T/T_c < 0.8$ deviated markedly from the WHH curve and showed saturation at $H = 52$ T, rather than at 92 T, a value which follows for data near T_c in accordance with the WHH theory. At $T = 0.38$ K, the $H^*_{c2\|ab}/H^*_{c2\perp ab}$ anisotropy was equal to 1.9.

Further evidence for concluding the orbital mechanism is insufficient to describe the behavior of the H^*_{c2} for a layered cuprate in a parallel magnetic field is obtained when we pass from a description in terms of H^*_{c2} to that in terms of the coherence length ξ in the anisotropic Ginzburg–Landau (GL) theory, under the assumption that the expressions linking H^*_{c2} and ξ are valid over a wide temperature range. Using the experimental data for H^*_{c2}, we found that the temperature dependence of the *ab*-plane coherence length $\xi_{ab}(T)$ was described well by GL theory, whereas the transverse coherence length ξ_c obtained from the data on $H^*_{c2\|ab}(T)$, was temperature-independent and very close to the *ab*-plane separation in Bi2201. The results obtained in a parallel magnetic field also disagree with theories assuming a 3D–2D crossover at low temperatures when the interlayer coupling vanishes. Our experiments evidenced no such crossover. We showed that the superconductivity of layered single crystals in a parallel magnetic field is limited by the paramagnetic effect, and applied the Ginzburg–Landau approximation to obtain

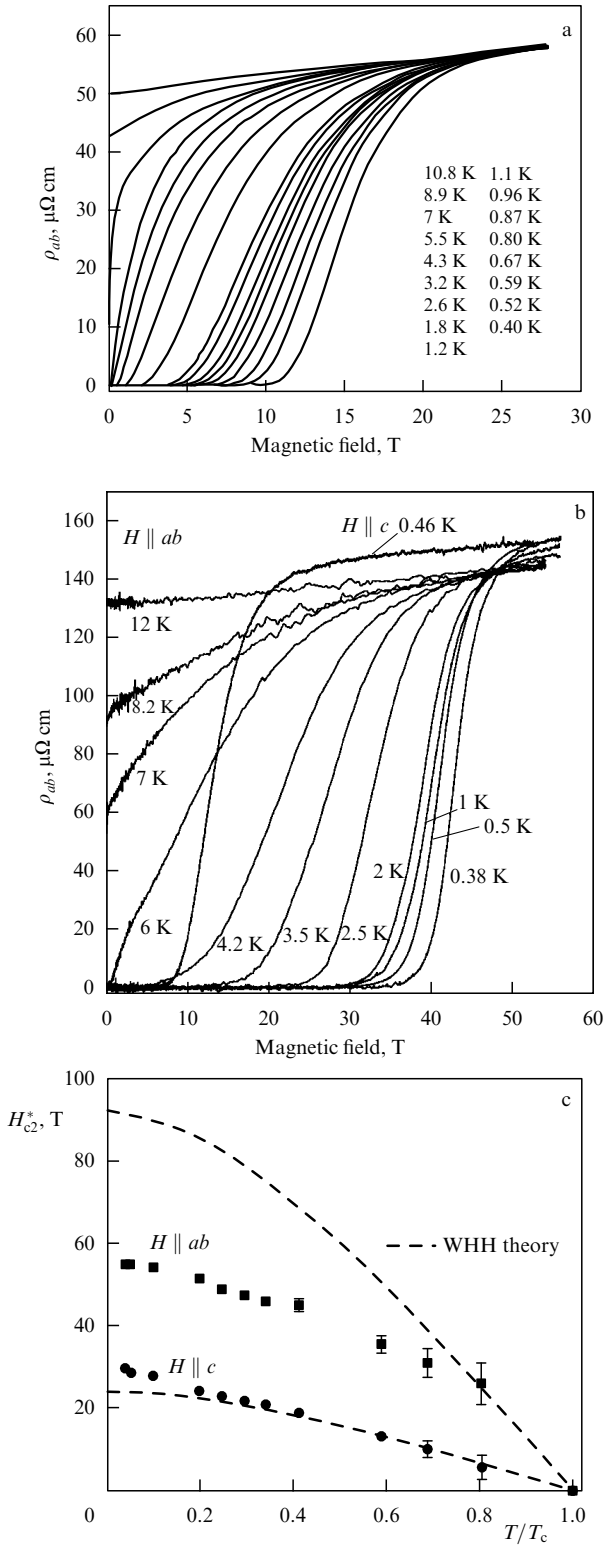

Figure 4. Diagrams illustrating the transition to the normal state in a Bi2201 single crystal in a magnetic field parallel to the *c*-axis (a) or *ab* plane (b) for different temperatures. (c) Resistive upper critical field H^*_{c2} (as determined from 100% normal-state resistivities shown in panels a and b) versus reduced temperature T/T_c for two field orientations, $H^*_{c2\perp ab}$ (circles) and $H^*_{c2\|ab}$ (squares). Dashed lines: WHH calculations [20, 21].

an expression for the paramagnetic limiting field, resulting in a value of $H^*_{c2\|ab}(0)$ close to the experimental one.

As noted above, an unusual feature of high-temperature superconductor properties in the normal state has to do with

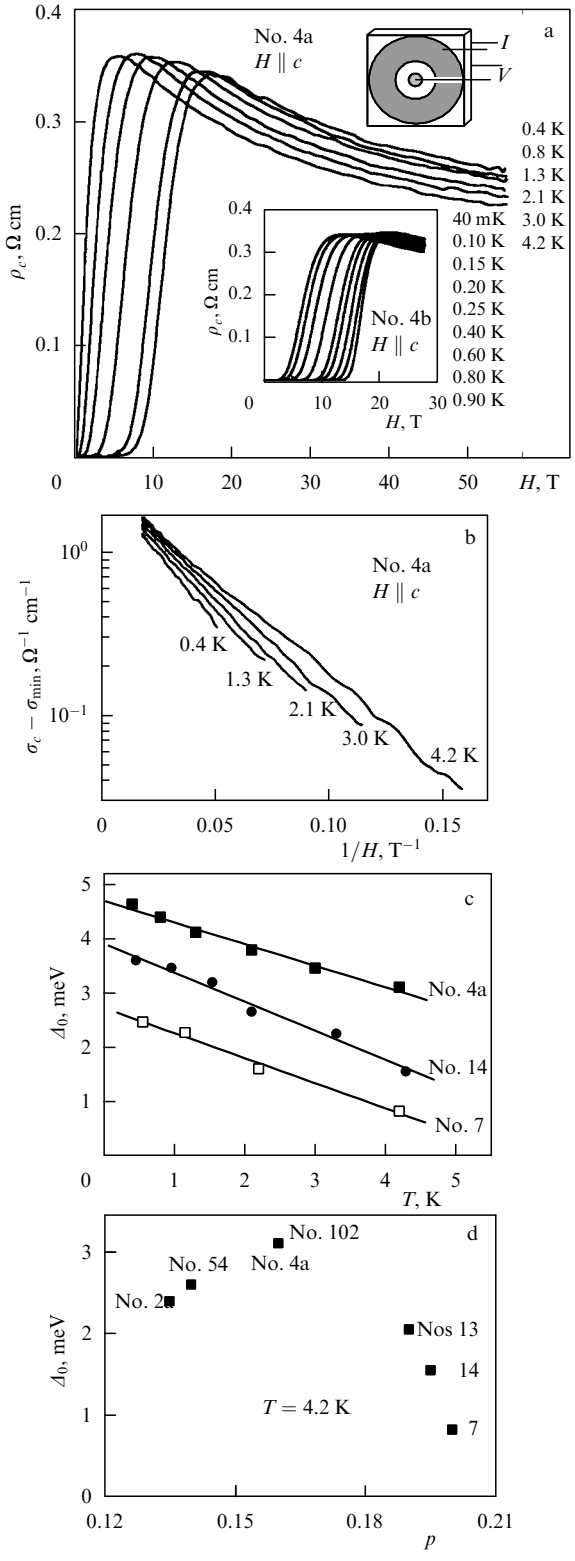

Figure 5. (a) Plot of $\rho_c(H)$ for temperatures 4.2–0.4 K in pulsed magnetic fields up to 55 T (sample 4a) for a Bi2201 single crystal with orientation $H^*_{c2\perp ab}$. Inset in the middle: the same for temperatures 0.9–0.04 K in constant magnetic fields up to 27 T (sample 4b). Upper right inset shows the arrangement of current and potential contacts. (b) Interlayer conductivity derived from data given in panel (a) on a semilog scale as a function of the inverse magnetic field for various temperatures. (c) Temperature dependence of the energy gap Δ_0 for three Bi2201 single crystals with different doping levels (0.16, 0.19, and 0.20). (d) Dependence of Δ_0 on doping level for different numbered Bi2201 samples [22].

the negative c-axis magnetoresistivity $\rho_c(H)$ which is observed in the temperature range of semiconducting $\rho_c(T)$ behavior and which some authors relate to the pseudogap. Figure 5a depicts such a $\rho_c(H)$ dependence for temperatures from 4.2 K to 0.4 K in pulsed magnetic fields up to 55 T; the inset shows $\rho_c(H)$ for a Bi2201 single crystal at temperatures of 0.90–0.04 K in constant magnetic fields up to 27 T. When the superconductivity of a sample is suppressed by an external magnetic field, its resistivity usually increases, reaches a maximum at a certain magnetic field H^c_p, and then decreases. The widespread belief has been that in the field H^c_p the sample changes to the normal state and that H^c_p is indentified with the upper critical field H_{c2}; the negative normal-state magnetoresistivity $\rho_c(H)$ was in this scenario thought to be due to a gradual closure of the pseudogap [23].

On the other hand, there was an attempt [2, 24, 25] to explain negative magnetoresistivity $\rho_c(H)$ by assuming that the interlayer conductivity in Bi2212 is governed by the sum of two processes proceeding in parallel: the Josephson tunneling and quasiparticle tunneling. Taken together, our experimental results on the megnetoresistivities $\rho_{ab}(H, T)$, $\rho_c(H, T)$ and interlayer magnetotunneling in Bi2201 single crystals evidenced that the Josephson component of the interlayer current vanishes at the maximum value of $\rho_c(H)$, leaving only quasiparticle tunneling (note that $H^c_p \ll H^*_{c2}$). We proved for the first time that spin correlations nonuniformly distributed in HTSC cuprates in the pseudogap state remain present even after superconductivity and local superconducting correlations have been suppressed. One recognizes the following four characteristic strengths of a magnetic field: $H^c_p < H^*_{c2} < H^{onset} < H^*$, where

(1) H^c_p suppresses phase coherence along the c-axis between superconducting CuO_2 layers (ab planes);

(2) H^*_{c2} establishes normal resistance in ab planes, i.e., suppresses phase coherence in CuO_2 layers;

(3) H^{onset} suppresses local superconducting correlations in noncoupled regions of the ab planes, and

(4) H^* is the field above which all spin-singlet correlations are destroyed.

Finally, we showed that in magnetic fields above H^c_p, the negative magnetoresistivity $\rho_c(H)$ of Bi2201 samples saturates exponentially with the growth in the magnetic field strength and that the interlayer conductivity of single crystals can be described by the functional in the form $\sigma_c = \sigma_0 \exp(-\Delta_0/g\mu_B H)$, where Δ_0 is a field-independent energy gap which we define as a pseudogap, or spin gap, and μ_B is the Bohr magneton. The slope of the linear dependence $\ln \sigma_c$ versus $1/H$ (Fig. 5b) gives Δ_0, and the change in the slope with temperature yields Δ_0 as a function of temperature. As seen from Fig. 5c, which presents data for three Bi2201 single crystals, this dependence is linear, with Δ_0 decreasing with increasing temperature. Moreover, it turned out that the value of Δ_0 is close to that of the superconducting gap and has a maximum (as a function of doping level) at the same value of p as T_c (Fig. 5d). In nonsuperconducting samples, one has $H^c_p = 0$ and $H^*_{c2} = 0$.

5. Superconducting gap and pseudogap of $Bi_2Sr_2CaCu_2O_{8+\delta}$ (Bi2212) single crystals as functions of the magnetic field

For simple superconductors, it is well known that a sufficiently strong magnetic field induces their transition to the normal state. The magnetic field suppresses superconduc-

tivity either as a result of the orbital effect, which destroys Cooper pairs, or through electron (Pauli) spin paramagnetism. These effects have been thoroughly studied in BCS superconductors. It is known, in particular, that in bulky samples the orbital effect is the dominant factor, whereas in thin films superconductivity is destroyed as a consequence of the Pauli effect. Both Ginzburg–Landau and BCS theories predict that the superconducting energy gap 2Δ in a magnetic field decreases with strengthening field, and vanishes when the field reaches H_{c2}. This prediction was confirmed, in particular, by tunneling spectroscopy which is the most informative tool for investigating superconductors, because the conductivity of a tunnel junction is directly proportional to the quasiparticle density of states.

Considerable evidence has been accumulated to show that the magnetic properties of HTSCs differ significantly from those of BCS superconductors. Naturally, the behavior of the superconducting gap in a magnetic field were also expected to be different. For example, it is commonly accepted that, unlike BCS superconductors, which exhibit an s symmetry, HTSCs possess a $d_{x^2-y^2}$ order-parameter symmetry, resulting in the superconducting gap possibly being dissimilar in different directions (see, for example, Ref. [26]). Although observed many times in tunneling experiments on Bi2212 samples, the energy gap evidenced no variations with magnetic field.

Nor were large gap variations observed in our preliminary work [27], a detailed, ultralow (30–50 mK) temperature field study up to 26 T of the quasiparticle density of states in Bi2212 single crystals using high-quality tunnel microcrack junctions (break type junctions). Nor, further, were we able to explain our results by either pure s pairing or pure $d_{x^2-y^2}$ pairing.

In recent angle-resolved photoemission spectroscopy (ARPES) studies of Bi2212 single crystals, a spectral gap was found near the nodal region in momentum space, which opened at T_c and had a near-BCS temperature dependence [28, 29] — in contrast to other directions, where the gap was less sensitive to T_c and varied in accordance with T^*. The fact that the ARPES temperature dependence of the spectral gap was observed to vary considerably along the Fermi surface allowed the hope that the magnetic field dependence of the energy gap will also be distinct at different points of the Fermi surface. Because rearrangement of our system of break junctions in liquid helium allowed a large number of tunnel junctions to be obtained at various locations of a microcrack in a single crystal, we made an attempt to find this gap and to examine its magnetic field dependence.

Figure 6a depicts the differential conductivities dI/dV of the tunnel junction as functions of the voltage bias V (all curves are shifted upward from the lowest one for clarity). The curves are typical for superconductor–insulator–superconductor tunnel junctions and are characterized by sharp peaks at $\pm V = 2\Delta/e$. The superconducting gap, defined as half of the separation between the main peaks, equals 45 meV at $T = 4.2$ K. Correspondingly, the reduced value of the gap width is $2\Delta/k_B T_c \simeq 6.2$. It is seen that, as the magnetic field strengthens, the main gap peaks in Fig. 6a decrease in amplitude and shift toward lower voltages. This behavior of the tunnel spectra can only be explained if the superconducting gap is suppressed by the magnetic field. Contrary to previous studies, where magnetic field has virtually no effect on the observed energy gap, we observed for the first time a superconducting gap which was suppressed considerably by a

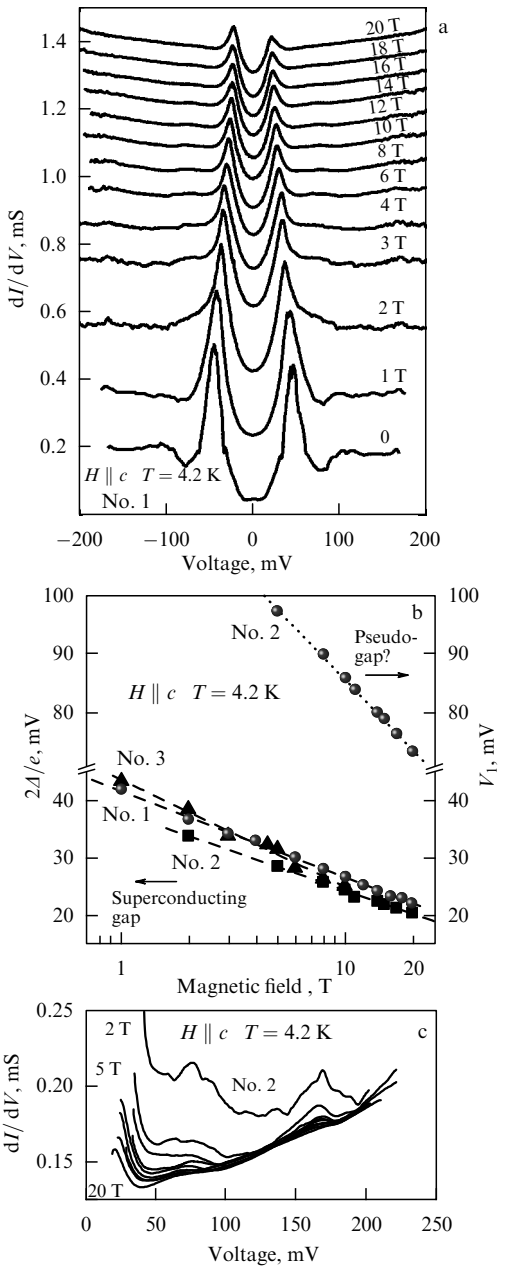

Figure 6. (a) Differential conductivity dI/dV as a function of voltage bias V for the tunnel break junction in a Bi2212 single crystal at $T = 4.2$ K for different magnetic fields parallel to the c-axis (for clarity, all curves are shifted upward from the lower curve). (b) Semilog plot of the magnetic field dependence of the superconducting gap width 2Δ calculated from data in panel (a). To illustrate the reproducibility of the field dependence of 2Δ, data from other tunnel junctions, obtained in other Bi2212 single crystals, are also shown. (c) Parts of the $dI/dV(V)$ dependence at a positive voltage bias above the gap maximum for a tunnel junction prepared in sample 2, for $T = 4.2$ K in various magnetic fields perpendicular to the *ab* plane [30].

magnetic field (to 50% at $H = 20$ T). This is a direct confirmation of the relationship between the discovered gap and superconductivity.

Figure 6b shows, based on Fig. 6a, a semilog plot of the energy gap 2Δ as a function of magnetic field strength for sample 1. To illustrate the reproducibility of the field dependence of 2Δ, tunnel junction data from single-crystalline Bi2212 samples 2 and 3 are also shown. It is seen that 2Δ decreases logarithmically with increasing magnetic field

(dashed lines), although we cannot rule out the possibility of an exponential dependence which also reasonably agrees with the experimental data. More importantly, the observed magnetic field dependence of 2Δ is inconsistent with the GL theoretical prediction that $\Delta(H) = \Delta(0)[1 - (H/H_{c2})^2]^{1/2}$, so that the superconducting gap should be nearly magnetic field-independent for $H \ll H_{c2}$ — in contrast to our twofold decrease.

Because estimates of the upper critical field H_{c2} for Bi2212 reside near 90 T [23], the magnetic field used in these experiments proved insufficient to suppress superconductivity at $T = 4.2$ K. This explains our observed reduction by as little as half in the superconducting gap width. To confirm that 2Δ remains logarithmic up to H_{c2} requires measurements in stronger magnetic fields, the more so since extrapolating the data in Fig. 6b linearly yields an unreasonably high value of hundreds of tesla for H_{c2}.

As seen from Fig. 6a, the tunneling spectra exhibit an additional noticeable structure at voltages above the main gap peaks. This dip-and-hump structure is a long-term subject of discussion, and it is as yet unclear whether it has some relation to the pseudogap or, as in simple superconductors, reflects strong coupling phenomena. Another evidence from Fig. 6a is the correlation between the dip and hump: as the magnetic field strengthens, they both are smeared, with their amplitudes rapidly decreasing, and follow simultaneously the gap peak in shifting toward lower voltages. This behavior is more clearly seen in Fig. 6c, which presents some portions of $dI/dV(V)$ dependences for a positive voltage bias above the gap peak for a tunnel junction in sample 2 for $T = 4.2$ K and different magnetic fields perpendicular to the *ab* plane. Of note is the fact that, as the magnetic field strength increases, the dip-and-hump structure moves to lower voltages much faster than the main peak related to the superconducting gap. Figure 6b displays the magnetic field dependence of the position V_1 of this structure on the voltage V_1-axis. This dependence was determined by measuring the second derivative $d^2I/dV^2(V)$, so that this dip-and-dump spectral structure cannot be linked to strong-coupling effects because, as its moves in a magnetic field simultaneously with the main gap peak, the difference between the peak and structure positions on the voltage axis should remain constant. Inspection of Fig. 6b shows, however, that this is not the case. A more reasonable conjecture seems to be that the dip-and-dump structure is related to a pseudogap which exists in a wide region of momentum space. The fact that the behavior of the gap and that of the dip-and-hump structure have different slopes in Fig. 6b indicates that the superconducting gap and pseudogap are affected differently by the magnetic field and suggests the absence of correlation between them in a Bi2212 cuprate.

Figure 6a, c shows yet another peak at a higher bias voltage, which is also smeared and decreases with the growth in the field, but, because its voltage-axis position is unchanged by the field, is likely to relate to an inelastic process in the tunnel barrier.

6. Conclusion

This paper briefly summarizes the results of magnetotransport and magnetotunneling studies done on single crystals of the high-temperature superconductors $Bi_{2+x}Sr_{2-x}CuO_6$ (Bi2201) and $Bi_2Sr_2CaCu_2O_8$ (Bi2212) in strong and ultrastrong magnetic fields in a wide temperature range down to 20 mK. In Bi2201 single crystal at $T \approx T_c$, the resistivity anisotropy is found to be $\rho_c/\rho_{ab} \approx 10^4$. At low temperatures, as the carrier concentration is decreased, Bi2201 in the normal state exhibits a metal–insulator transition. In the $T \to 0$ limit, the charge transfer mechanism is the same in the *ab* plane and along the *c*-axis (anisotropic three-dimensional behavior). The Wiedemann–Franz law holds for pure optimally doped Bi2201 single crystals but starts to break down as the doping levels are decreased in the vicinity of the metal–insulator transition. The elementary excitations that transfer charge and heat in cuprates are fermions. Given the resistance anisotropy in Bi2201, it follows from the anisotropic Ginzburg–Landau relation that the anisotropy of the upper critical field H^*_{c2} should be approximately 100, whereas, in fact, the $H^*_{c2\parallel ab}/H^*_{c2\perp ab}$ anisotropy at $T = 0.38$ K turned out to be 1.9. At low temperatures, due to Pauli paramagnetism, the external magnetic fields needed to destroy superconductivity exceed 30 T. There are four characteristic magnetic field strengths in HTSC cuprates: $H_p^c < H^*_{c2} < H^{onset} < H^*$. The superconducting gap and pseudogap in HTSCs significantly depend on the magnetic field, although in a different way.

References

1. Martin S et al. *Phys. Rev. B* **41** 846 (1990)
2. Briceno G, Crommie M F, Zettl A *Phys. Rev. Lett.* **66** 2164 (1991)
3. Forro L *Phys. Lett. A* **179** 140 (1993)
4. Ono S et al. *Phys. Rev. Lett.* **85** 638 (2000)
5. Ando Y et al. *Phys. Rev. Lett.* **77** 2065 (1996); *Phys. Rev. Lett.* **79** 2595 (1997), Erratum
6. Anderson P W *Phys. Rev.* **109** 1492 (1958)
7. Emery V J, Kivelson S A *Nature* **374** 434 (1995)
8. Hotta T, Mayr M, Dagotto E *Phys. Rev. B* **60** 13085 (1999)
9. Maly J, Jankó B, Levin K *Phys. Rev. B* **59** 1354 (1999)
10. Gorina J et al. *Solid State Commun.* **91** 615 (1994)
11. Martovitsky V P, Gorina J I, Kaljushnaia G A *Solid State Commun.* **96** 893 (1995)
12. Vedeneev S I, Maude D K *Phys. Rev. B* **70** 184524 (2004)
13. Jing T W et al. *Phys. Rev. Lett.* **67** 761 (1991)
14. Ando Y et al. *Phys. Rev. Lett.* **75** 4662 (1995)
15. Hill R W et al. *Nature* **414** 711 (2001)
16. Bel R et al. *Phys. Rev. Lett.* **92** 177003 (2004)
17. Proust C et al. *Phys. Rev. B* **72** 214511 (2005)
18. Mackenzie A P et al. *Phys. Rev. Lett.* **71** 1238 (1993)
19. Osofsky M S et al. *Phys. Rev. Lett.* **71** 2315 (1993)
20. Vedeneev S I et al. *Phys. Rev. B* **60** 12467 (1999)
21. Vedeneev S I et al. *Phys. Rev. B* **73** 014528 (2006)
22. Vedeneev S I et al. *Phys. Rev. B* **75** 064512 (2007)
23. Shibauchi T et al. *Phys. Rev. Lett.* **86** 5763 (2001)
24. Gray K E, Kim D H *Phys. Rev. Lett.* **70** 1693 (1993)
25. Morozov N et al. *Phys. Rev. Lett.* **84** 1784 (2000)
26. Won H, Maki K *Phys. Rev. B* **49** 1397 (1994)
27. Vedeneev S I, Maude D K *Phys. Rev. B* **72** 144519 (2005)
28. Lee W S et al. *Nature* **450** 81 (2007)
29. Chien C-C et al. *Phys. Rev. B* **79** 214527 (2009)
30. Vedeneev S I, Piot B A, Maude D K *Phys. Rev. B* **81** 054501 (2010)